ACS APPLIED MATERIALS & INTERFACES

Research Article

www.acsami.org

Near-Infrared Emitting Fluorescent BODIPY Nanovesicles for in Vivo Molecular Imaging and Drug Delivery

Li Quan,[∥,†] Shi Liu,[∥,†] Tingting Sun,[†,§] Xingang Guan,[†] Wenhai Lin,[†,§] Zhigang Xie,*[,†] Yubin Huang,[†] Yiqing Wang,[‡] and Xiabin Jing[†]

[†]State Key Laboratory of Polymer Physics and Chemistry, Changchun Institute of Applied Chemistry, Chinese Academy of Sciences, Changchun 130022, China

[‡]Department of Biomedical Engineering, College of Modern Engineering and Applied Sciences, Nanjing University, Nanjing 210093, China

[§]University of Chinese Academy of Sciences, Beijing 100049, China

Supporting Information

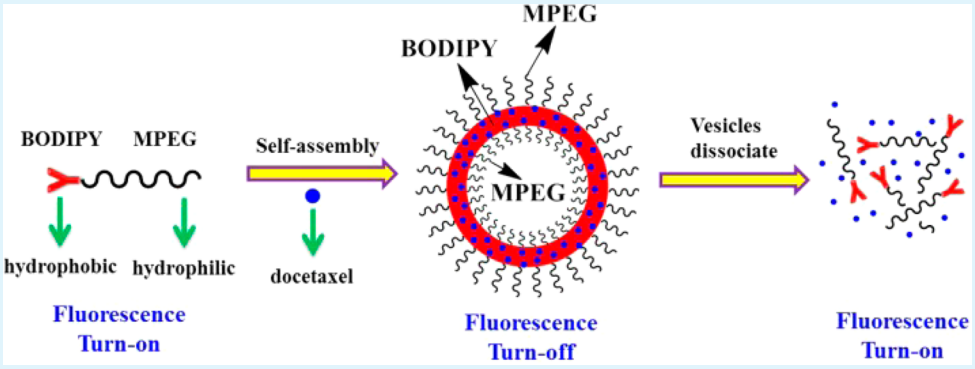

ABSTRACT: Near-infrared fluorescent nanovesicles were prepared by self-assembly of block copolymer hydrophilic poly(ethylene glycol) boron−dipyrromethenes in aqueous solution. The fluorescence enhancement induced by dissociation of nanovesicles could be used as a smart imaging and diagnostic tool. This nanovesicle could encapsulate the antitumor drug, and provide a powerful platform for imaging-guided tumor-specific drug delivery and therapy.

KEYWORDS: *nanovesicles, near-infrared, BODIPY, in vivo imaging, drug delivery*

1. INTRODUCTION

Polymeric nanoparticles (NPs) have been of significant interest for application in medical diagnosis and therapeutics.[1,2] For example, amphiphilic copolymers could self-assembly in aqueous solution to form nanoscale micelles or vesicles that can encapsulate drugs and deliver them to a diseased target. Recent clinical studies have proved that polymeric NPs incorporating anticancer drugs will lead to better tumor regression compared to free drugs.[3] Fluorescent molecules are suitable models to prove the successful encapsulation and to allow for tracking the fate of NPs in vivo.[4−6] Particularly, near-infrared (NIR) emissions are especially suitable in diagnosis and therapy-diagnosis because of their ability of penetrating the skin and underlying tissue with low background interference.

The NIR fluorescent dyes currently used in biomedical imaging analysis include the following two categories: traditional organic NIR dyes and NIR fluorescent nanomaterials. The former includes cyanine dyes,[7,8] dye-containing tetrapyrroles,[9] and thiazide/oxazine dyes.[10−12] Many of such dyes have obvious shortcomings, such as poor light stability, small Stokes shift, and poor water solubility. Typical examples of NIR fluorescent nanomaterials are semiconductor quantum dots (QD)[13] and single-walled carbon nanotubes (SWNT).[14,15] However, their disadvantages are also obvious, for example, existence of toxic heavy metal ions and "luminous blinking" in QDs, or low fluorescence quantum yield and easy aggregation (accompanied by fluorescence quenching) of SWNT, which greatly limit biological application.[16−18] Boron−dipyrromethenes (BODIPY), as a new family of fluorescent dye, tend to be strongly UV-absorbing small molecules that emit relatively sharp fluorescence peaks with high quantum yields and stability in physiological conditions.[19−22] There have been many reports on BODIPY fluorescent dyes in the past decades,[23−26] but few of them are water-soluble and can emit at more than 650 nm, while water solubility and NIR fluorescence are essential requirements for imaging in living cells and whole animals.

Several strategies have been developed to incorporate both fluorescent dyes and therapeutic drugs into nanostructures,

Received: June 30, 2014
Accepted: August 27, 2014
Published: August 27, 2014

Scheme 1. Synthesis of Amphiphilic Polymer mPB Based on the NIR BODIPY and Preparation of Its Vesicular NPs

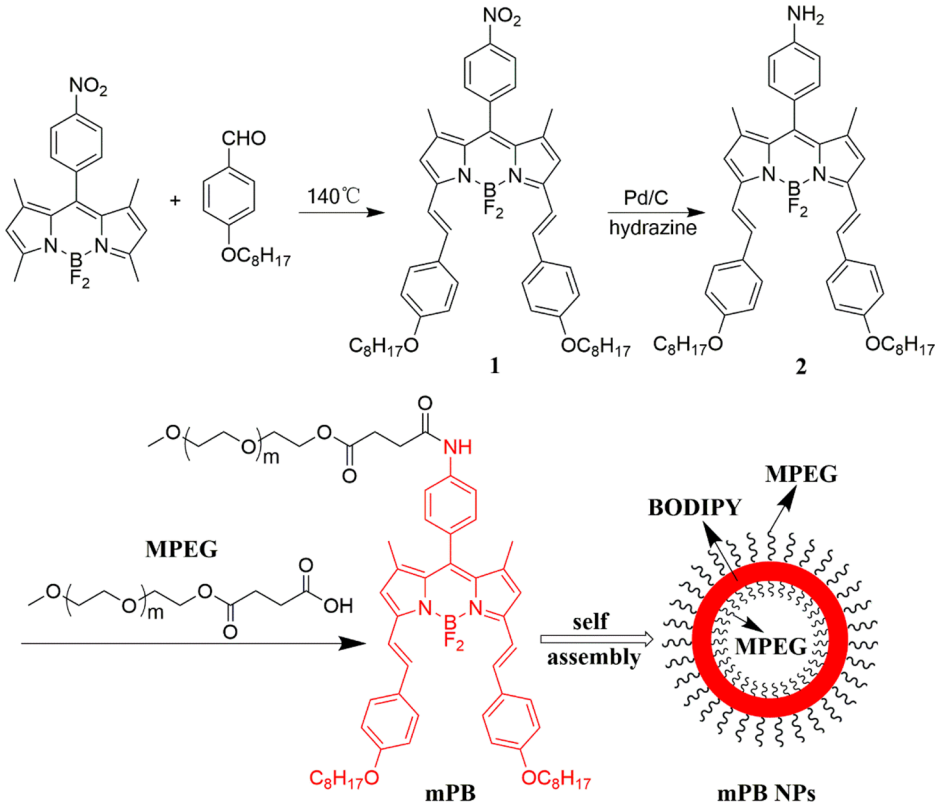

including physical encapsulation or chemical modification.[27] These strategies usually need multistep or complicated procedures. It is highly desirable to develop a simple and universal polymeric vehicle for both drug and fluorescent dyes. Amphiphilic molecules for preparation of nanoparticles could be made by conjugation of dye molecules to the MPEG. Although some work has been reported in recent years,[28−30] the nanovesicles containing NIR fluorescence is seldom seen in literature. Herein, we made an amphiphilic fluorescent macromolecule MPEG-BODIPY (mPB) by conjugating NIR BODIPY with hydrophilic poly(ethylene glycol) (MPEG) (Scheme 1). The mPB was able to self-assemble into polymeric nanoparticles (NPs) with 57 nm aqueous solution, which could also encapsulate hydrophobic or hydrophilic drugs. The NIR mPB NPs less than 100 nm are important for their passive targeting in tumor site. As a result, such vesicles are both therapeutic and diagnostic because of the coincorporation of anticancer drugs and NIR BODIPY moieties in general. In particular, the NIR BODIPY moieties in the NPs are in the aggregated state and thus fluoresce weakly due to the aggregation quenching effect. Once the NPs are dissociated for some reasons, the NIR dyes become intensely fluorescent. As dissociation of mPB NPs is usually accompanied by drug release, the fluorescence measurement will reveal the place and velocity of the drug release in vivo from mPB vesicles. Furthermore, as a simple conjugate of MPEG and NIR BODIPY, mPB does not contain other hydrophobic segments and the NIR BODIPY plays a role of fluorophore, hydrophobic moiety, and carrier of hydrophobic drugs.

2. RESULTS AND DISCUSSION

As shown in Scheme 1, a highly hydrophobic NIR BODIPY dye (compound **1**) with relatively large molecular weight (801 g mol^{-1}) was synthesized by reacting 4-nitro-phenyl-BODIPY[30,31] with 4-octyloxybenzaldehyde[32] via condensation reaction. Under catalysis of Pd/C, compound **1** was reduced to compound **2** in the presence of hydrazine hydrate. The structures of compound **1** and **2** were confirmed by ^{1}H NMR spectra, matrix-assisted laser desorption/ionization time-of-flight mass spectrometry (MALDI-TOF MS), and elemental analysis (see Supporting Information, Figures S6−S10). The UV−vis absorption and fluorescence emission showed the λ_{max} of compound **1** (640 and 670 nm) and **2** (643 and 673 nm) in dimethylformamide (DMF) are almost with the peak shape and position of the same. An amphiphilic molecule mPB was obtained by reaction of carboxyl mPEG$_{5000}$ (methoxy-poly-(ethylene glycol, molecular weight 5000) and compound **2**. Thin-layer chromatography (TLC) was used to monitor the reaction progress until the starting material was completely consumed. On the basis of the complete solubility of mPEG in water and the amphiphilic nature of mPB, dialysis against water was used to prepare the NPs of mPB and to remove the residual mPEG left in the reaction system. The BODIPY content in the mPB NPs was estimated to be 0.13 mg BODIPY per milligram NPs by ultraviolet visible (UV−vis) spectroscopy (Supporting Information, Figure S1a). Appearance of the Fourier transform infrared (FT-IR) spectroscopy peaks at 1650 and 1513 cm^{-1} related to the amide I and amide II modes were indicative of successful bonding of NIR-BODIPY onto the PEG terminal through amide bonds (Supporting Information, Figure S1b).

To prepare NPs of mPB, its tetrahydrofuran (THF) solution was added into deionized water and then tetrahydrofuran (THF) was evaporated. A hollow-sphere morphology with a diameter range of 50−80 nm was observed by transmission electron microscopy (TEM) (Figure 1a) and the average

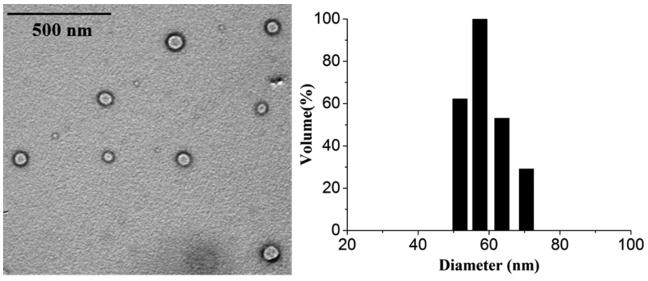

Figure 1. TEM image (a) and size distribution (b) of self-assembly of mPB in water determined by DLS.

hydrodynamic diameter determined by dynamic light scattering (DLS) was 57 ± 10 nm (Figure 1b). On the basis of the PEGylated block copolymers, it is reported that a ratio of 35 ± 10% of the hydrophilic segment to the total mass of the amphiphile is a boundary between polymeric micelles and vesicles.[33,34] In the present case, the hydrophilic mPEG segment took about 87 wt % of the total mass of mPB, but vesicles with hollow cavity were formed. This unusual formation of mPB vesicles in water was ascribed to the strong hydrophobicity and a large conjugated rigid planar structure of the BODIPY dye. Obviously, this vesicle morphology provides three possibilities: (1) hydrophobic drugs can be encapsulated into the BODIPY layer of the vesicle; (2) hydrophilic drugs can be captured in the inner cavity of the vesicle; (3) both hydrophobic and hydrophilic drugs can be incorporated into the vesicles to achieve combination therapy. In short, the mPB vesicles are promising drug delivery vehicles as well as a fluorescent label.

The fluorescence of mPB NPs in water and DMF was examined. As shown in Figure 2a, mPB NPs did not show fluorescence at all in water but gave strong NIR fluorescence in DMF. This indicates that fluorescence quenching took place in a mPB vesicle in aqueous solution because of the aggregation of BODIPY molecules. When the vesicle dissociated in DMF, fluorescence was recovered. In addition, the DMF solution of mPB exhibited maximum absorption and emission peaks at 643 and 673 nm (Figure 2c), respectively, which were the same as those of free BODIPY in DMF (Figure 2b). It is obvious that coupling of BODIPY onto the MPEG terminal did not bring significant change to its fluorescence character.

The above results indicated that aggregation state plays a key role in the fluorescence of mPB NPs. The fluorescence of mPB NPs was examined in vitro under different conditions: 1) in phosphate buffer solution (PBS) at pH = 7.4 (mimicking normal tissues); 2) in fetal bovine serum (FBS, blood circulation); 3) in PBS at pH = 5.0 (tumor environment). The fluorescence intensity at 673 nm (I_{673}) almost kept constant (Figure 3a) at pH = 7.4, whereas it increased with time in phosphate buffered saline (PBS) of pH 5.0 or in fetal bovine serum (FBS) (Figure 3b,c). Seen from Figure 3d, the mPB vesicles were stable up to 180 h in PBS of pH 7.4 but dissociated under acidic conditions or in FBS. These results show that fluorescence enhancement of mPB NPs could be used for studying the stability of the aggregates and tracking the fate of NPs in vivo, especially when drugs are encapsulated inside the vesicles.

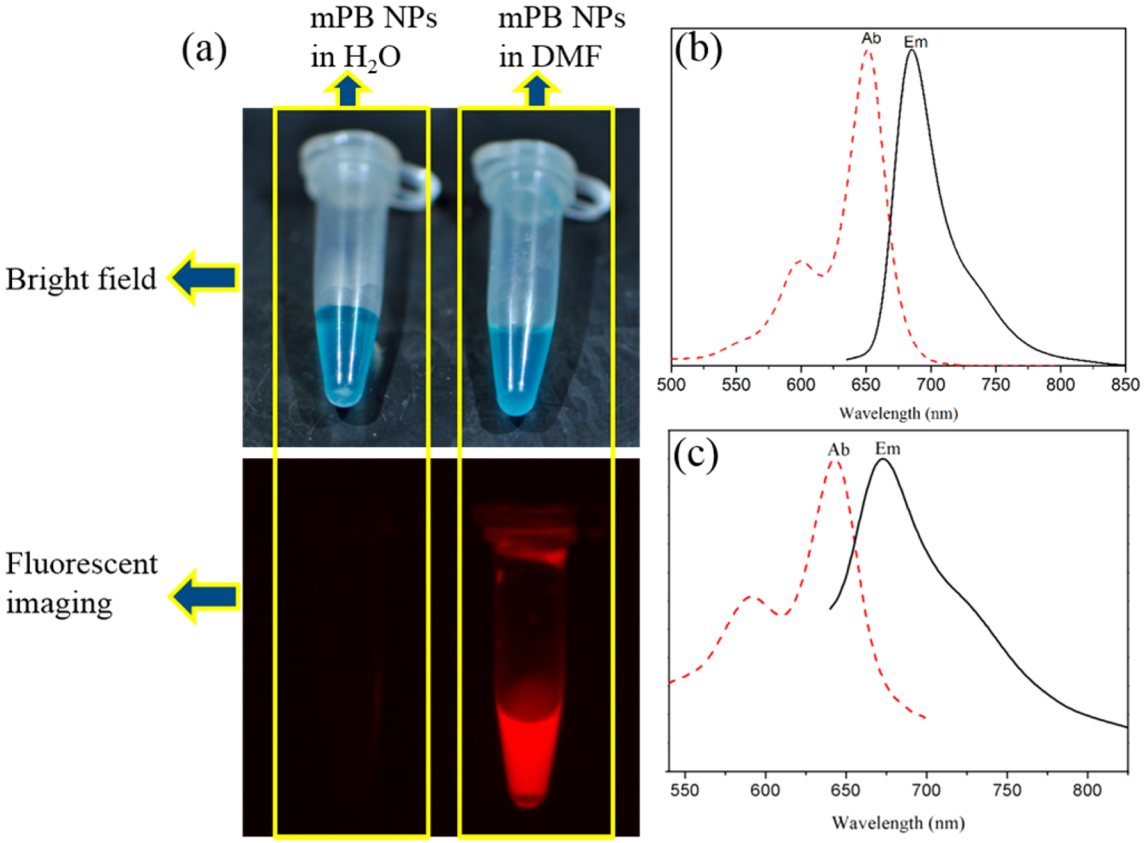

Figure 2. (a) Fluorescence of mPB NPs in water and in DMF solution: bright field and fluorescent photos; (b and c) normalized fluorescent spectra of free NIR BODIPY (ε = 929 M^{-1} cm^{-1}, Φ = 0.08) and mPB in DMF solution (ε = 24 062 M^{-1} cm^{-1}, Φ = 0.21).

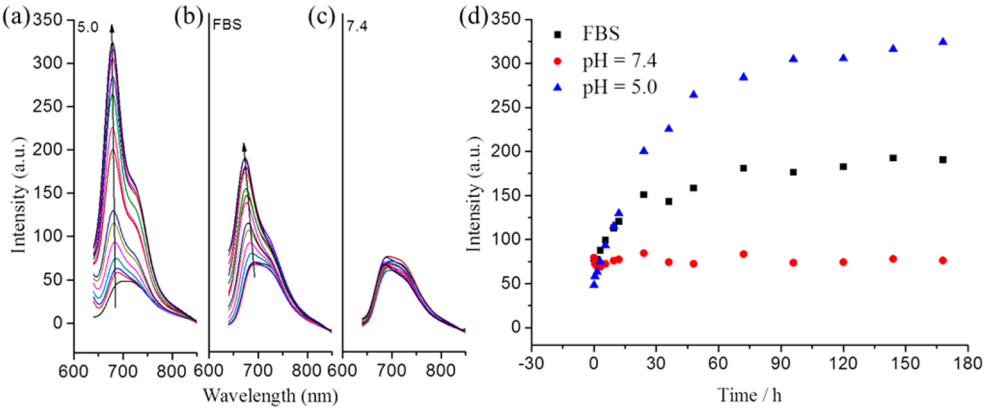

Figure 3. Emission spectra of mPB in different environments over time at 37 °C. (a) In PBS, pH = 5.0; (b) in FBS; (c) in PBS, pH = 7.4; (d) plots of fluorescence intensity of mPB (λ_{673}) with various times in different environments.

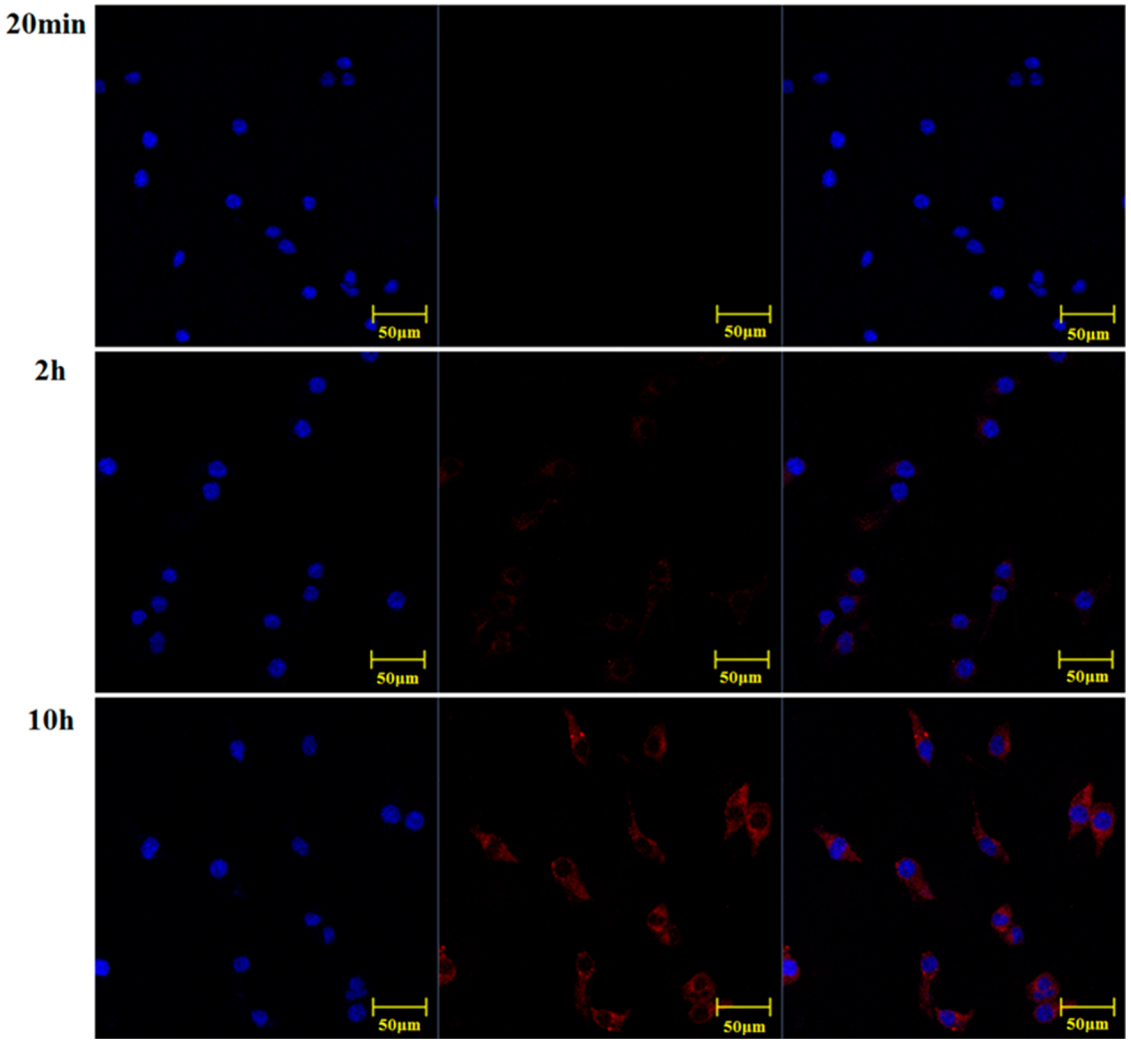

Figure 4. CLSM images of HepG-2 cells treated with mPB NPs in PBS (pH 7.4) (content of NIR BODIPY 0.01 mg mL^{-1}) for various times and the nucleus was labeled with 2-(4-amidinophenyl)-6-indolecarbamidine (DAPI); the fluorescent images were obtained via a Zeiss confocal laser microscope (ZEISS LSM 700). Left panel, DAPI image; middle panel, BODIPY image; right panel, overlay of the both.

The biocompatibility of nanomaterials is very important for their biomedical applications. Herein, the biocompatibility of mPB was evaluated using HepG-2 cells. As shown in Figure S2 (Supporting Information), no obvious cytotoxicity was observed even at a concentration of 200 μg/mL for mPB after 24 h. To monitor destiny of the mPB NPs in living cells, HepG-2 cells were incubated with mPB vesicles in PBS of pH 7.4 and examined by confocal laser scanning microscopy (CLSM). As shown in Figure 4, in the first 20 min, no NIR fluorescence was observed. As time went on, the NIR

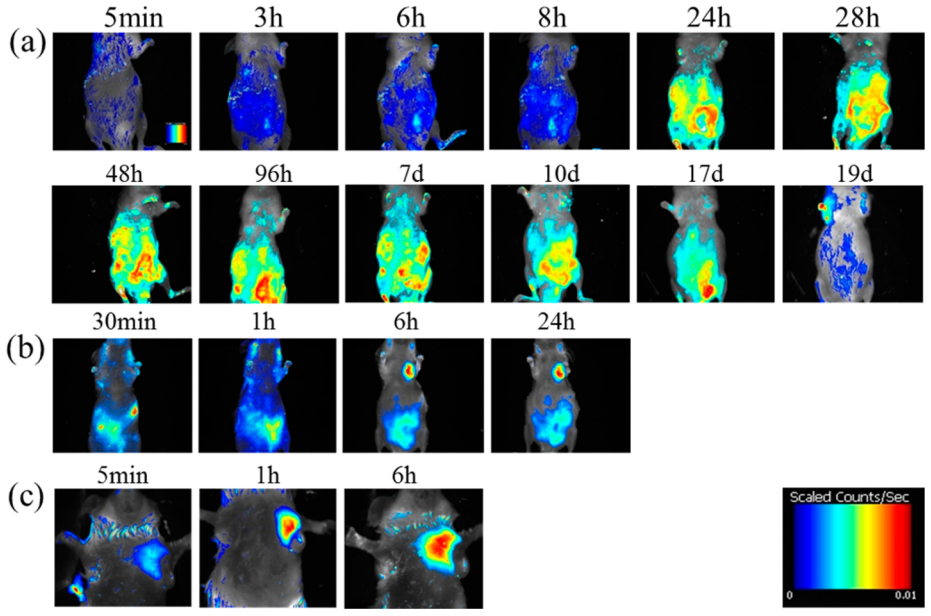

Figure 5. In vivo NIR fluorescence imaging of hair-removed mice: (a) healthy mice after tail-vein injection of mPB solution for different time intervals; (b) mice bearing H22 tumor in the armpit after tail-vein injection of mPB solution; (c) mice bearing H22 tumor in the armpit after intratumor injection of mPB solution. In all cases, the equivalent NIR BODIPY dose was 2.0 μg per mouse.

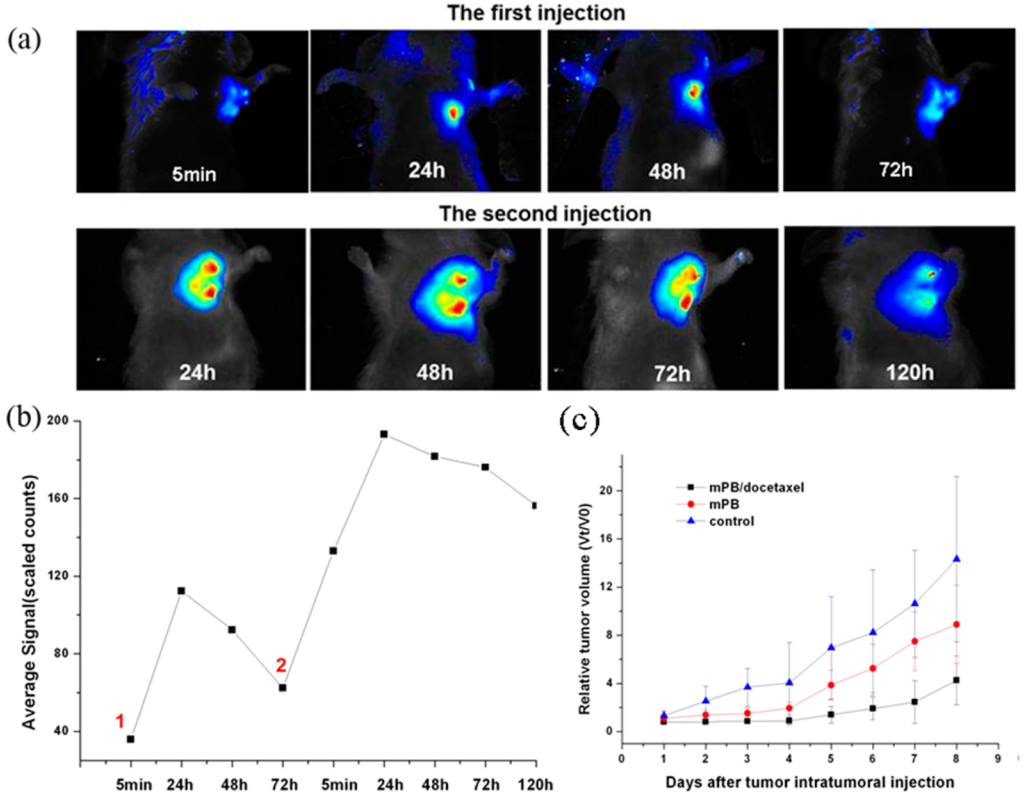

Figure 6. In vivo fluorescence images of mouse bearing H22 liver cancer after intralesional injection of mPB/docetaxel. (a and b) In vivo NIR fluorescence imaging and semiquantitative fluorescence intensities of the tumor area determined at different times. Red numbers indicate the twice injections; (c) relative tumor volume of H22 xenograft model as a function of time: "control" stands for the natural growth of tumor; "mPB" and "mPB/docetaxel" stand for the growth of tumor after injection of blank mPB NPs and mPB/docetaxel, respectively. V0 means tumor volume at day 0 and Vt means tumor volume at different time points. Each data point represents the average of five samples and error bars represent standard deviation (n = 5).

fluorescence became stronger and stronger. At 10 h, the NIR fluorescence was full of the cell plasma. According to our previous results in this study, only dissociated dye molecules can fluoresce. The observed NIR fluorescence in Figure 4 means that the mPB NPs can be internalized by the HepG-2 cells and the internalized mPB NPs need time to disintegrate to

dx.doi.org/10.1021/am5042115 | ACS Appl. Mater. Interfaces 2014, 6, 16166−16173

show their NIR fluorescence. In contrast, when a solution of free NIR BODIPY in mixture solvent (dimethyl sulfoxide:water =1:9, v/v) was prepared and the HepG-2 cells were treated with this solution for 2 h, no NIR fluorescence from the cells was observed (Supporting Information, Figure S3). This means that free NIR BODIPY cannot be internalized efficiently by the cells because of its high level of hydrophobicity.

NIR fluorescence imaging, with advantages of high tissue penetration and low autofluorescence,[35] could be used for noninvasively tracking the tumor-specific delivery and biodistribution. Herein, we examined the fluorescence of mPB vesicles after they were injected in living body by a Maestro 500FL in vivo optical imaging system (Cambridge Research & Instrumentation, Inc., USA) under excitation with yellow light (575−605 nm). First, normal Kunming mice were tested. 200 μL of mPB NPs water-solution with a concentration of 0.01 mg mL^{-1} of NIR BODIPY was intravenously injected via the tail-vein, and animals were imaged at multiple time points (Figure 5a). Due to their circulation and dissociation in the body, an increasingly stronger fluorescence signal was observed until 48 h. Then fluorescence became weaker and weaker possibly due to metabolism. After 19 days, these mPB were almost completely metabolized. The normal animal experiment indicated that NIR mPB is low toxicity in tested mice. H22 (hepatocarcinoma 22 cell line) xenograft models were established by subcutaneous inoculation in the armpit of Chinese Kunming mice. After the H22 tumors grew to about 8−10 mm in diameter, 200 μL of NP solution (content of NIR BODIPY 0.01 mg mL^{-1}) was injected via tail-vein. It is well-known that NPs in vivo are absorbed more easily by the liver, kidney, and spleen. At 0.5 h, considerable fluorescence signals were observed there. And over time, the fluorescence became weaker due to circulation and metabolism in the body. Meanwhile, the fluorescence coming from the tumor site was visible at 1 h, and became stronger than that in the abdominal area at 6 h (Figure 5**b**). This was attributed to passive targeting based on the enhanced permeability and retention (EPR) effect because of their small size of 57 nm.[36] This result implied that the mPB NPs had accumulated in the cancer site and got disintegrated there. In comparison, intratumoral injection was carried out. As shown in Figure 5c, only 5 min after injection, a significant fluorescent signal was detected, and the fluorescent signal increased gradually over time, and did not spread to other parts of the body. This rapid disintegration in the cancer site and reproducible tumor-targeted accumulation are suggestive of diagnostic agent of mPB NPs for tumors.

To prepare anticancer drug-carrying mPB NPs, a similar procedure was used with a mixture solution in THF of mPB and docetaxel as starting materials for self-assembling in water. TEM observation confirmed the vesicle morphology and DLS measurement gave its size of 85 ± 18 nm (Supporting Information, Figure S4). Compared with mPB vesicles in Figure 1, the increasing size and contrast in TEM images is due to the incorporating of docetaxel in the mPB vesicles, which also indicated the successful encapsulation of decetaxel. The docetaxel content of the mPB/docetaxel NPs obtained was 9.1 wt % determined by HPLC. Then, the fluorescence of mPB/docedaxel NPs under different conditions was examined. mPB/docetaxel NPs displayed much more intense fluorescence in THF than in water (data not shown). As shown in Figure S5 (Supporting Information), its fluorescence intensity increased with time in FBS, similar to the case of mPB vesicles in various media (Figures 2 and 3). This means that encapsulation of antitumor drug did not affect the fluorescence behaviors. Finally, in vivo examination was carried out in Kunming mice with H22 liver cancer. The mouse was injected with mPB/docetaxel (0.5 mg mL^{-1} of docetaxel, 20 μL) at the center of the tumor, and then imaged at different time points. As shown in Figure 6a,b, in the first minutes after injection, mPB/docetaxel NPs were located at the injection site but did not show intense fluorescence because they were in the vesicle state. Then the fluorescence became stronger and stronger in the first hours, indicating disintegration of the vesicles and release of docetaxel from the vesicles. After 24 h postinjection, the fluorescence intensity of the tumor area gradually decayed with time due to the metabolism. After 72 h, the fluorescence signal was relatively weak. The second injection was performed, and the fluorescent intensity went through another procedure of strengthening (within 24 h) and weakening (after 24 h) (Figure 6b). Until over 120 h a weak fluorescence signal was still observed, implying some of mPB remained at the tumor site. As pointed out earlier, fluorescence of mPB is associated with the disintegration of mPB vesicles and the release of decetaxel. Such released docetaxel would play its role as antitumor agent. As shown in Figure 6c, indeed, tumor growth was inhibited by mPB/docetaxel in comparison with the control group and mPB NPs. This result implies that we can track the drug movement and drug release by virtue of the NIR fluorescence enhancement.

3. CONCLUSIONS

In summary, fluorescent nanovesicles were prepared by self-assembling of amphiphilic MPEG-BODIPY molecules in aqueous solution. Their fluorescence enhancement based on the dissociation of NPs could be used in bioimaging in vitro and vivo. The nanoscale vesicles show low toxicity and high accumulation in tumor site through passive targeting. Encapsulation of antitumor drug decetaexl using nanovesicles was obtained via self-assembly method. In vivo experiments indicated mPB/docetaxel NPs possess excellent intratumor imaging and tumor inhibition. The NIR NPs provide a useful platform for imaging-guided drug delivery and cancer therapy.

4. MATERIALS AND METHODS

All starting materials were purchased from Aldrich and Fisher, unless otherwise noted. ^{1}H NMR spectra were recorded on a Bruker NMR 400 DRX spectrometer at 400 MHz and referenced to the proton resonance resulting from incomplete deuteration of deuterated chloroform (δ 7.26). UV−vis absorption spectra were obtained using a Shimadzu UV-2450 PC UV−vis spectrophotometer. Strengthening experiments were performed using PerkinElmer LS-55 spectrofluorophotometer. The size and distribution of particles were determined by the dynamic light scattering at 25 °C with the scattering angle 90° and vertical polarization He−Ne laser (DAWN EOS, Wynatt Technology). The mass spectra (MS) of samples were recorded by the German company Bruker autoflex III smartbeam MALDI-TOF/TOF mass spectrometer with smartbeam laser at 355 nm wavelength. The morphology of particles were obtained using transmission electron microscopy (TEM) JEOL JEM-1011 (Japan) at the accelerating voltage of 100 kV. The emission quantum yields in DMF were obtained relative to rhodamine 6G at room temperature. Docetaxel content was determined by analyzing samples using HPLC (LC-10ATvp, Shimadzu) with a eluent of mixture of methanol, acetonitrile and water (CH_3OH:CH_3CN:H_2O = 0.25:0.25:0.5, v/v/v). The column effluent at 14.1 min was detected at 230 nm.

4.1. Synthesis of NIR BODIPY. Compound **1**: The starting materials *meso*-nitro-phenyl-BODIPY and 4-octyloxybenzaldehyde were synthesized according to the references.[37−39] The *meso*-nitro-

phenyl-BODIPY (200 mg, 0.54 mmol), 4-octyloxybenzaldehyde (507 mg, 2.17 mmol, 4 equiv), and PTSA (p-toluenesulfonamide) (5 mg, 0.03 mmol) were dissolved in toluene (25 mL) and piperidine (1 mL) in a round-bottom flask equipped with a Dean−Stark apparatus. The resulting solution was heated at 140 °C until all the solvents were collected by the Dean−Stark apparatus. Toluene (25 mL) and piperidine (1 mL) were added to the solid reaction media and the drying protocol was repeated four times. Purification by chromatography on silica gel (1:3 dichloromethane/petroleum ether) afforded a dark solid (0.25 g, 57%). ^{1}H NMR (300 MHz, $CDCl_3$): δ = 8.40 (d, J = 12.2 Hz, 2H), 7.82 (d, J = 6.5 Hz, 2 H), 7.51 (d, J = 6.6 Hz, 4 H), 7.25 (d, J = 12.2 Hz, 2 H), 6.72 (d, J = 6.6 Hz, 4H), 6.45 (d, J = 6.5 Hz, 2H), 6.39 (s, 2 H), 3.60 (m, 4H), 1.32−1.18 (m, 18 H), 1.12 (s, 6H), 0.92 (s, 6H), 0.49 (s, 6H); TOF MS m/z (nature of the peak) calcd: 801.81. Found: 801.5 [M^+]. Calcd for $C_{49}H_{58}BF_2N_3O_4$: C 73.40, H 7.92, N 5.24. Found: C 73.18, H 8.26, N 5.07.

Compound **2**: compound **1** was dissolved in warm THF (30 mL). Ethanol (30 mL) was added as a cosolvent. After purged with N_2, 10% Pd/C (1.0 g) and 1.0 mL hydrazine were added. The solution was stirred at reflux under N_2 for 30 min, cooled to 20 °C, and poured into water. The aqueous mixture was extracted with CH_2Cl_2. The extract was washed with water, and the solvent was removed on a rotary evaporator. The residue was taken up in CH_2Cl_2 and applied to a silica gel column chromatography using hexane/CH_2Cl_2 (1:2) to afford the desired compound NIR BODIPY (0.11 g, 46%). ^{1}H NMR (300 MHz, $CDCl_3$): δ = 8.44 (d, J = 12.4 Hz, 2H), 7.50 (d, J = 6.5 Hz, 4 H), 7.24 (d, J = 12.4 Hz, 4 H), 6.71 (d, J = 6.5 Hz, 4 H), 6.57 (d, J = 6.2 Hz, 2H), 6.44 (s, 2 H), 6.19 (d, J = 6.2 Hz, 2 H), 3.61 (m, 4H), 1.40−1.23 (m, 30 H), 0.91 (m, 6H); TOF MS m/z (nature of the peak) calcd: 771.83. Found: 771.6 [M^+]. Calcd for $C_{49}H_{60}BF_2N_3O_2$: C 76.25, H 7.84, N 5.44. Found: C 76.08, H 8.06, N 5.21.

4.2. Synthesis of Carboxyl mPEG$_{5000}$. Briefly, to a solution of mPEG$_{5000}$ (5 mmol) in 30 mL $CHCl_3$ was added succinic anhydride (6.25 mmol) and pyridine (0.5 mL) and the reaction mixture was stirred at 60 °C for 48 h. The reaction mixture was concentrated under reduced pressure, and the product was added with saturated solution of $NaHCO_3$ (20 mL) and acidized to pH = 2 by 2 mol L^{-1} of hydrochloric acid. It was thereafter extracted with chloroform, followed by drying with anhydrous magnesium sulfate, concentration, and precipitation with ether to gain a white solid (11.3 g, 45%).

4.3. Synthesis of mPB. To a stirred solution of NIR BODIPY (771 mg, 1 mmol), carboxyl mPEG$_{5000}$ (6.5 g, 1.3 mmol) in CH_2Cl_2 (30 mL), *N*,*N*′-dicyclohexylcarbodiimide (206 mg, 1 mmol) and 4-dimethylaminopyrridine (122 mg, 1 mmol) were added at 0 °C, and stirring was continued at 0 °C for 2 h. Stirring continued for 48 h at room temperature, and the reaction mixture was filtered. It was thereafter precipitated with ether to gain a black-blue solid (3.94 g, 78%).

4.4. Preparation of mPB NPs. First, 10 mg of mPB was dissolved in 5 mL of tetrahydrofuran, and then was slowly dripped into 10 mL of water. Under the rapid mixing, THF was slowly evaporated, and a clear blue water solution remained. To remove the residual mPEG left in the reaction system, the solution was dialyzed against water for 2 days.

4.5. In Vitro Cell Imaging. HepG-2 cells were precultured in 6-well plates (Costar, IL, USA) containing cell culture coverslips to achieve 80% confluence (cell number 5×10^5/well). The medium was then removed and the cells were washed twice with 2× PBS buffer, followed by addition of 100 μL water solution of NPs (content of NIR BODIPY 10^{-5} mol L^{-1}) or mixture solution (DMSO:H_2O = 1:9, v/v) of free BODIPY (content of NIR BODIPY 10^{-5} mol L^{-1}) into fresh DMEM for incubation at 37 °C. At different time points, the cell monolayer was washed using 2× PBS buffer and fixed using 4% paraformaldehyde for 10 min. The coverslips were sealed with mounting medium and the confocal images were obtained using Zeiss confocal laser microscope (ZEISS LSM 700).

4.6. Preparation of mPB/Docetaxel NPs. First, 9 mg of mPB and 1 mg of docetaxel was dissolved in 5 mL of tetrahydrofuran, and then was slowly dripped into 10 mL of water. Under the rapid mixing, THF was slowly evaporated. The unincorportated docetaxel was removed by filtering with a synring filter (pore size: 0.45 μm) and the mPB/decetaxel NPs were obtained by freeze-drying. Docetaxel content was determined by high performance liquid chromatography (HPLC).

4.7. In Vivo Fluorescence Imaging and Cancer Treatment. All animal experiments were performed complying with the NIH guidelines for the care and use of laboratory animals. The xenograft tumors were established by subcutaneously injecting H22 cells into the armpit of Kunming mice. After tumors of 8−10 mm in diameter were palpable, whole body images of mice were acquired respectively by a tail vein injection and intratumoral injection of 200 μL of mPB NPs at a concentration of 0.01 mg mL^{-1}. In addition, whole body images of healthy mice were acquired after a tail-vein injection of 200 μL of mPB NPs at a concentration of 0.01 mg mL^{-1}. All images were analyzed and collected at the indicated time points with an in vivo imaging system (Maestro emission filter, Longpass: 645 nm cut-in, Part No. MK50102-Yellow; Maestro excitation filter, Bandpass: 575−605 nm, Part No. MK50102-Yellow). For the tumor treatment, the animals were randomly divided into three groups with five mice in each groups and treated with mPB NPs or mPB/docetaxel. Tumor length and width were measured with calipers. The tumor volume was calculated using the equation: tumor volume (V) = length × width^2/2.

■ ASSOCIATED CONTENT

Ⓢ Supporting Information

The standard curve of mPB; FT-IR of mPB; the biocompatibility of mPB; CLSOM images of BODIPY at various times; morphologies and size of mPB/doxcetaxel; the emission of mPB/doxcetaxel in different environments over time; ^{1}H NMR and MALDI-TOF of BODIPY. This material is available free of charge via the Internet at http://pubs.acs.org.

■ AUTHOR INFORMATION

Corresponding Author

*Z. Xie. Fax: +86-431-85262779. E-mail: xiez@ciac.ac.cn.

Author Contributions

‖The paper was written through contributions of all authors. All authors have given approval to the final version of the paper. L. Quan and S. Liu contributed equally.

Notes

The authors declare no competing financial interest.

■ ACKNOWLEDGMENTS

This work was financially supported by China Postdoctoral Science Foundation (No. 2013M540260), the National Natural Science Foundation of China (Project Nos. 91227118 and 21104075).

■ REFERENCES

(1) Davis, M. E.; Chen, Z.; Shin, D. M. Preorganized, Macromolecular, Gene-Delivery Systems. *Nat. Rev. Drug Discovery* **2008**, *7*, 771−782.

(2) Shi, J.; Votruba, A. R.; Farokhzad, O. C.; Langer, R. Nanotechnology in Drug Delivery and Tissue Engineering: From Discovery to Applications. *Nano Lett.* **2010**, *10*, 3223−3230.

(3) Matsumura, Y.; Kataoka, K. Preclinical and Clinical Studies of Anticancer Agent-Incorporating Polymer Micelles. *Cancer Sci.* **2009**, *100*, 572−579.

(4) Liu, G. Y.; Liu, X. S.; Wang, S. S.; Chen, C. J.; Ji, J. Biomimetic Polymersomes as Carriers for Hydrophilic Quantum Dots. *Langmuir* **2012**, *28*, 557−562.

(5) Hauschild, S.; Lipprandt, U.; Rumplecker, A.; Borchert, U.; Rank, A.; Schubert, R.; Forster, S. Direct Preparation and Loading of Lipid and Polymer Vesicles Using Inkjets. *Small* **2005**, *1*, 1177−1180.

(6) Discher, B. M.; Won, Y. Y.; Ege, D. S.; Lee, J. C. M.; Bates, F. S.; Discher, D. E.; Hammer, D. A. Polymersomes: Tough Vesicles Made from Diblock Copolymers. *Science* **1999**, *284*, 1143−1146.

(7) Escobedo, J. O.; Rusin, O.; Lim, S.; Strongin, R. M. Near-Infrared Molecular Probes for in Vivo Imaging. *Curr. Opin. Chem. Biol.* **2010**, *14*, 64−70.
(8) Chen, X. Q.; Nam, S. W.; Kim, G. H.; Song, N.; Jeong, Y.; Shin, I.; Kim, S. K.; Kim, J.; Park, S.; Yoon, J. A Near-Infrared Fluorescent Sensor for Detection of Cyanide in Aqueous Solution and Its Application for Bioimaging. *Chem. Commun.* **2010**, *46*, 8953−8955.
(9) Leevy, W. M.; Gammon, S. T.; Jiang, H.; Johnson, J. R.; Maxwell, D. J.; Jackson, E. N.; Marquez, M.; Piwnica-Worms, D.; Smith, B. D. Optical Imaging of Bacterial Infection in Living Mice Using a Fluorescent Near-Infrared Molecular Probe. *J. Am. Chem. Soc.* **2006**, *128*, 16476−16477.
(10) Umezawa, K.; Matsui, A.; Nakamura, Y.; Citterio, D.; Suzuki, K. Bright, Color-Tunable Fluorescent Dyes in the Vis/NIR Region: Establishment of New "Tailor-Made" Multicolor Fluorophores Based on Borondipyrromethene. *Chem.—Eur. J.* **2009**, *15*, 1096−1106.
(11) Umezawa, K.; Nakamura, Y.; Makino, H.; Citterio, D.; Suzuki, K. Bright, Color-Tunable Fluorescent Dyes in the Visible−Near-Infrared Region. *J. Am. Chem. Soc.* **2008**, *130*, 1550−1551.
(12) Rao, J. H.; Dragulescu-Andrasi, A.; Yao, H. Q. Fluorescence Imaging in Vivo: Recent Advances. *Curr. Opin. Biotechnol.* **2007**, *18*, 17−25.
(13) Chan, W. C. W.; Maxwell, D. J.; Gao, X. H.; Bailey, R. E.; Han, M. Y.; Nie, S. M. Luminescent Quantum Dots for Multiplexed Biological Detection and Imaging. *Curr. Opin. Biotechnol.* **2002**, *13*, 40−46.
(14) Choi, H. S.; Ipe, B. I.; Misra, P.; Lee, J. H.; Bawendi, M. G.; Frangioni, J. V. Tissue- and Organ-Selective Biodistribution of NIR Fluorescent Quantum Dots. *Nano Lett.* **2009**, *9*, 2354−2359.
(15) Welsher, K.; Liu, Z.; Daranciang, D.; Dai, H. J. Selective Probing and Imaging of Cells with Single Walled Carbon Nanotubes as Near-Infrared Fluorescent Molecules. *Nano Lett.* **2008**, *8*, 586−590.
(16) Hoyer, P.; Staudt, T.; Engelhardt, J.; Hell, S. W. Quantum Dot Blueing and Blinking Enables Fluorescence Nanoscopy. *Nano Lett.* **2011**, *11*, 245−250.
(17) Lee, A. J.; Wang, X. Y.; Carlson, L. J.; Smyder, J. A.; Loesch, B.; Tu, X. M.; Zheng, M.; Krauss, T. D. Bright Fluorescence from Individual Single-Walled Carbon Nanotubes. *Nano Lett.* **2011**, *11* (4), 1636−1640.
(18) Boghossian, A. A.; Zhang, J. Q.; Barone, P. W.; Reuel, N. F.; Kim, J. H.; Heller, D. A.; Ahn, H. J.; Hilmer, A. J.; Rwei, A.; Arkalgud, J. R.; Zhang, C. T.; Strano, M. S. Near-Infrared Fluorescent Sensors Based on Single-Walled Carbon Nanotubes for Life Sciences Applications. *ChemSusChem.* **2011**, *4*, 848−863.
(19) Quan, L.; Lin, W. H.; Sun, T. T.; Xie, Z. G.; Huang, Y. B.; Jing, X. B. Green Photocatalysis with Oxygen Sensitive BODIPYs under Visible Light. *Catal. Lett.* **2014**, *144*, 308−313.
(20) Quan, L.; Chen, Y.; Lv, X. J.; Fu, W. F. Aggregation-Induced Photoluminescent Changes of Naphthyridine−BF_2 Complexes. *Chem.—Eur. J.* **2012**, *18*, 14599−14604.
(21) Loudet, A.; Burgess, K. BODIPY Dyes and Their Derivatives: Syntheses and Spectroscopic Properties. *Chem. Rev.* **2007**, *107*, 4891−4932.
(22) Smith, A. M.; Mancini, M. C.; Nie, S. M. Bioimaging: Second Window for in Vivo Imaging. *Nat. Nanotechnol.* **2009**, *4*, 710−711.
(23) Worries, H. J.; Koek, J. H. A Novel Water-Soluble Fluorescent Probe: Synthesis, luminescence and Biological Properties of the Sodium Salt of the 4-Sulfonato-3,3′,5,5′-tetramethyl-2,2′-pyrromethen-1,1′-BF_2 complex. *Recl. Trav. Chim. Pays-Bas* **1985**, *104*, 288−291.
(24) Karolin, J.; Johansson, L. B. A.; Strandberg, L.; Ny, T. Fluorescence and Absorption Spectroscopic Properties of Dipyrrometheneboron Difluoride (BODIPY) Derivatives in Liquids, Lipid Membranes, and Proteins. *J. Am. Chem. Soc.* **1994**, *116*, 7801−7806.
(25) Tan, K.; Jaquinod, L.; Paolesse, R.; Nardis, S.; Di Natale, C.; Di Carlo, A.; Prodi, L.; Montalti, M.; Zaccheroni, N.; Smith, K. M. Synthesis and Characterization of β-Fused Porphyrin-BODIPY® Dyads. *Tetrahedron* **2004**, *60*, 1099−1106.
(26) Wagner, R. W.; Lindsey, J. S. Boron-Dipyrromethene Dyes for Incorporation in Synthetic Multi-Pigment Light-Harvesting Arrays. *Pure Appl. Chem.* **1996**, *68*, 1373−1380.
(27) Johnston, A. P. R.; Such, G. K.; Ng, S. L.; Caruso, F. Challenges Facing Colloidal Delivery Systems: From Synthesis to the Clinic. *Curr. Opin. Colloid Interface Sci.* **2011**, *16*, 171−181.
(28) Feng, X.; Lv, F.; Liu, L.; Tang, H.; Xing, C.; Yang, Q.; Wang, S. Conjugated Polymer Nanoparticles for Drug Delivery and Imaging. *ACS Appl. Mater. Interfaces* **2010**, *2*, 2429−2435.
(29) Zhang, C.; Jin, S.; Li, S.; Xue, X.; Liu, J.; Huang, Y.; Jiang, Y.; Chen, W.-Q.; Zou, G.; Liang, X.-J. Imaging Intracellular Anticancer Drug Delivery by Self-Assembly Micelles with Aggregation-Induced Emission (AIE Micelles). *ACS Appl. Mater. Interfaces* **2014**, *6*, 5212−5220.
(30) Guo, J.; Hong, H.; Chen, G.; Shi, S.; Nayak, T. R.; Theuer, C. P.; Barnhart, T. E.; Cai, W.; Gong, S. Theranostic Unimolecular Micelles Based on Brush-Shaped Amphiphilic Block Copolymers for Tumor-Targeted Drug Delivery and Positron Emission Tomography Imaging. *ACS Appl. Mater. Interfaces* **2014**, *6*, ASAP.
(31) Levine, D. H.; Ghoroghchia, P. P.; Freudenberg, J.; Zhang, G.; Therien, M. J.; Greene, M. I.; Hammer, D. A.; Murali, R. Polymersomes: A New Multi-Functional Tool for Cancer Diagnosis and Therapy. *Methods* **2008**, *46*, 25−32.
(32) Rodriguez-Hernandez, J.; Checot, F.; Gnanou, Y.; Lecommandoux, S. Toward "Smart" Nano-Objects by Self-Assembly of Block Copolymers in Solution. *Prog. Polym. Sci.* **2005**, *30*, 691−724.
(33) Liu, G. Y.; Chen, J. C.; Ji, J. Biocompatible and Biodegradable Polymersomes as Delivery Vehicles in Biomedical Applications. *Soft Matter* **2012**, *8*, 8811−8821.
(34) Xiao, H.; Song, H.; Yang, Q.; Wang, R.; Xie, Z.; Huang, Y.; Li, Y.; Wu, Y.; Jing, X. The Use of Polymeric Platinum(IV) Prodrugs to Deliver Multinuclear Platinum(II) Drugs with Reduced Systemic Toxicity and Enhanced Antitumor Efficacy. *Biomaterials* **2012**, *33*, 8657−8669.
(35) Gao, F.; Li, L.; Fu, C.; Nie, L.; Chen, D.; Tang, F. LHRH-PE40 Fusion Protein Tethered Silica Nanorattles for Imaging-Guided Tumor-Specific Drug Delivery and Bimodal Therapy. *Adv. Mater.* **2013**, *25*, 5508−5513.
(36) Cabral, H.; Matsumoto, Y.; Mizuno, K.; Chen, Q.; Murakami, M.; Kimura, M.; Terada, Y.; Kano, M. R.; Miyazono, K.; Uesaka, M.; Nishiyama, N.; Kataoka, K. Accumulation of Sub-100 nm Polymeric Micelles in Poorly Permeable Tumours Depends on Size. *Nat. Nanotechnol.* **2011**, *6*, 815−823.
(37) Pez, D.; Leal, I.; Zuccotto, F.; Boussard, C.; Brun, R.; Croft, S. L.; Yardley, V.; Ruiz Perez, L. M.; Gonzalez Pacanowska, D.; Gilbert, I. H. 2,4-Diaminopyrimidines as Inhibitors of Leishmanial and Trypanosomal Dihydrofolate Reductase. *Bioorg. Med. Chem.* **2003**, *11*, 4693−4711.
(38) Li, M.; Wang, H.; Zhang, X.; Zhang, H. Development of A New Fluorescent Probe: 1,3,5,7-Tetramethyl-8-(4′-Aminophenyl)-4,4-difluoro-4-bora-3a,4a-diaza-s-Indacence for the Determination of Trace Nitrite. *Spectrochim. Acta, Part A* **2004**, *60*, 987−993.
(39) Olivier, J. H.; Widmaier, J.; Ziessel, R. Near-Infrared Fluorescent Nanoparticles Formed by Self-Assembly of Lipidic (Bodipy) Dyes. *Chem.—Eur. J.* **2011**, *17*, 11709−11714.